

Minerva Access is the Institutional Repository of The University of Melbourne

Author/s:

Jackson, TD;Cramer, JJ;Muellner-Wong, L;Frazier, AE;Palmer, CS;Formosa, LE;Hock, DH;Fujihara, KM;Stait, T;Sharpe, AJ;Thorburn, DR;Ryan, MT;Stroud, DA;Stojanovski, D

Title:

Sideroflexin 4 is a complex I assembly factor that interacts with the MCIA complex and is required for the assembly of the ND2 module

Date:

2022-03-29

Citation:

Jackson, T. D., Cramer, J. J., Muellner-Wong, L., Frazier, A. E., Palmer, C. S., Formosa, L. E., Hock, D. H., Fujihara, K. M., Stait, T., Sharpe, A. J., Thorburn, D. R., Ryan, M. T., Stroud, D. A. & Stojanovski, D. (2022). Sideroflexin 4 is a complex I assembly factor that interacts with the MCIA complex and is required for the assembly of the ND2 module. *Proceedings of the National Academy of Sciences of the United States of America*, 119 (13), <https://doi.org/10.1073/pnas.2115566119>.

Persistent Link:

<https://hdl.handle.net/11343/327050>

License:

[CC BY-NC-ND](#)



Sideroflexin 4 is a complex I assembly factor that interacts with the MCIA complex and is required for the assembly of the ND2 module

Thomas D. Jackson^{a,b}, Jordan J. Cramer^{a,b}, Linden Mueller-Wong^{a,b,c}, Ann E. Frazier^{c,d}, Catherine S. Palmer^{a,b}, Luke E. Formosa^e, Daniella H. Hock^{a,b}, Kenji M. Fujihara^{f,g}, Tegan Stait^{c,h}, Alice J. Sharpe^e, David R. Thorburn^{c,d,h}, Michael T. Ryan^e, David A. Stroud^{a,b,c}, and Diana Stojanovski^{a,b,1}

Edited by Peter Rehling, University of Goettingen, Goettingen, Germany; received August 26, 2021; accepted February 11, 2022 by Editorial Board Member Ulrich Hartl

Sideroflexins (SFXNs) comprise a family of five paralogous proteins (SFXN1–5) in metazoan species. SFXN1/2/3 function as mitochondrial serine transporters and are required for efficient mitochondrial one-carbon (1C) metabolism. SFXN4 is evolutionarily divergent, and mutations in *SFXN4* give rise to mitochondrial disease, pointing to a distinct function of this protein in mitochondrial biology. Using a combination of genome editing, interaction studies, and quantitative proteomics, we show that loss of SFXN4 leads to an isolated complex I assembly defect and that SFXN4 interacts with the core components of the mitochondrial complex I intermediate assembly (MCIA) complex. Our findings suggest that SFXN4 is required for the incorporation of the mtDNA-encoded ND6 subunit in the ND2 assembly module of complex I. These findings provide insights into the fundamental process of complex I assembly and functional insights into a disease-causing gene belonging to the SFXN family.

mitochondria | respiratory chain | complex assembly | sideroflexins

Mitochondria house numerous metabolic pathways, including the ATP-producing electron transport chain, and regulate signaling pathways responsible for activities including antiviral defense and programmed cell death (1). Reflecting their functional complexity, mitochondria possess two membranes and are host to a large repertoire of proteins (2), which are encoded by both the nuclear and the mitochondrial genomes. Despite dramatic increases in knowledge of mitochondrial biology, many of the 1,136 high-confidence mitochondrial proteins (2) remain partially or fully uncharacterized (3).

Sideroflexins (SFXNs) are a family of inner membrane proteins that are evolutionarily distinct from the SLC25A mitochondrial carrier family, although both protein families utilize the TIM22 complex for insertion into the inner membrane (4). Of the five SFXN members, SFXN1 and SFXN3 (and, potentially, SFXN2) function as serine transporters and are required for mitochondrial one-carbon metabolism (5). It has also been suggested that SFXN1 is required to maintain complex III integrity (6). Kory and colleagues showed that the most divergent member of the SFXN family, SFXN4, has no serine transport capacity (5). Mutations in *SFXN4* cause a mitochondrial disease (OMIM 615578) with clinical features including macrocytic anemia and a deficiency in complex I of the mitochondrial electron transport chain (7, 8).

Complex I exists in the inner mitochondrial membrane, comprises 45 subunits, and is assembled through an intricate pathway that brings together several independently assembled modules (9, 10). Complex I subunits are encoded by both the nuclear and the mitochondrial genomes, necessitating a tightly regulated assembly pathway. This pathway is assisted by multiple assembly factors, which interact with complex I subunits and assembly intermediates during the assembly process, but are absent in the mature complex (9, 10). For example, the mitochondrial complex I intermediate assembly (MCIA) complex (11)—harboring the assembly factors NDUFAF1, ECSIT, ACAD9, TMEM126B, TMEM186, and COA1—is required for building the ND2 membrane module that contains the mitochondrial DNA (mtDNA) encoded subunits ND2, ND3, ND4L, and ND6 along with six nuclear encoded subunits (9, 10, 12, 13). Complex I further associates with other respiratory chain enzymes (complexes III and IV) during assembly to form the respirasome, the functional significance of which is highly debated (14–16).

The evolutionary divergence of SFXN4, its inability to transport serine, and its clinical association with complex I deficiency and mitochondrial disease raised the hypothesis that SFXN4 has a distinct function to other SFXN proteins, likely linked to

Significance

Mitochondria are double-membraned eukaryotic organelles that house the proteins required for generation of ATP, the energy currency of cells. ATP generation within mitochondria is performed by five multisubunit complexes (complexes I to V), the assembly of which is an intricate process. Mutations in subunits of these complexes, or the suite of proteins that help them assemble, lead to a severe multisystem condition called mitochondrial disease. We show that SFXN4, a protein that causes mitochondrial disease when mutated, assists with the assembly of complex I. This finding explains why mutations in *SFXN4* cause mitochondrial disease and is surprising because SFXN4 belongs to a family of amino acid transporter proteins, suggesting that it has undergone a dramatic shift in function through evolution.

Author contributions: T.D.J., D.A.S., and D.S. designed research; T.D.J., J.J.C., L.M.-W., A.E.F., C.S.P., L.E.F., D.H.H., T.S., and A.J.S. performed research; D.R.T., M.T.R., and D.S. contributed new reagents/analytic tools; T.D.J., J.J.C., L.M.-W., A.E.F., D.H.H., K.M.F., D.A.S., and D.S. analyzed data; and T.D.J. and D.S. wrote the paper.

The authors declare no competing interest.

This article is a PNAS Direct Submission. P.R. is a guest editor invited by the Editorial Board.

Copyright © 2022 the Author(s). Published by PNAS. This article is distributed under Creative Commons Attribution-NonCommercial-NoDerivatives License 4.0 (CC BY-NC-ND).

¹To whom correspondence may be addressed. Email: d.stojanovski@unimelb.edu.au.

This article contains supporting information online at <http://www.pnas.org/lookup/suppl/doi:10.1073/pnas.2115566119/-DCSupplemental>.

Published March 25, 2022.

complex I biogenesis. We show that cells lacking *SFXN4* present with an isolated complex I assembly defect, and functional analysis of *SFXN4* uncovered extensive interactions with the MCIA complex. The association of *SFXN4* with MCIA guides assembly of the ND2 module of complex I, and we show that *SFXN4* interacts with newly synthesized ND6, one of the last subunits to be added to this module. Our data show that *SFXN4* is a complex I assembly factor, which interacts with the MCIA complex and acts in ND2-module maturation by integrating mtDNA-encoded ND6.

Results

Deletion of *SFXN4* Results in Isolated Complex I Deficiency.

To explore possible functions for *SFXN4*, we analyzed the Achilles gene essentiality dataset to identify genes that were coessential with *SFXN4* (17, 18). Several of the genes that had the highest coessentiality with *SFXN4* were complex I subunits or assembly factors (Fig. 1*A*), or other components of the OXPHOS (oxidative phosphorylation) system (Fig. 1*B*), suggesting that *SFXN4* functions in complex I biogenesis. Coessentiality with complex I or the mitochondrial OXPHOS system more broadly was not observed for *SFXN1*, *SFXN2*, *SFXN3*, or *SFXN5* (*SI Appendix, Fig. S1 A and B*), confirming that this association is unique to *SFXN4* and is a reflection of the protein's divergent molecular function.

To interrogate the function of *SFXN4* in detail, we generated a *SFXN4* knock-out (*SFXN4*^{KO}) HEK Flp-InTM T-RexTM cell line using CRISPR-Cas9 gene editing (*SI Appendix, Fig. S1C*). Mitochondria were isolated from control and *SFXN4*^{KO} cells and were analyzed by label-free quantitative mass spectrometry (MS) (Fig. 1*C* and *SI Appendix, Table S1*). *SFXN4*^{KO} cells were depleted of a number of complex I subunits (Fig. 1*C* and *SI Appendix, Table S1*), with proteins belonging to the N (NDUFA7, NDUFS1, NDUFV1), Q (NDUFA9) and ND2 (NDUFA10) assembly modules of complex I being the most significantly affected. Consistent with the proteomic data, sodium dodecyl sulfate–polyacrylamide gel electrophoresis (SDS-PAGE) analysis confirmed the ND2 module subunit NDUFA10 and the Q module subunit NDUFA9 were depleted in *SFXN4*^{KO} cells, while the abundance of the ND4 module subunit NDUFB11 was unchanged (Fig. 1*D*). The proteomics and SDS-PAGE data indicated the OXPHOS defect in *SFXN4*^{KO} cells was specific to complex I, as levels of subunits belonging to complexes II, III, IV, or V remained unchanged (Fig. 1*C–E*). Topographical heat mapping of the relative subunit abundances from the proteomics dataset onto a recent cryoelectron microscopy–derived structure of complex I highlighted how the observed changes corresponded to distinct complex I assembly modules (Fig. 1*F*). Together, these data suggested the lack of *SFXN4* in mitochondria results in a specific defect in complex I assembly and/or stability.

We monitored complex I assembly and respiratory chain integrity in control and *SFXN4*^{KO} cells using Blue-Native (BN) PAGE of mitochondria solubilized in digitonin (maintains supercomplexes) or Triton X-100 (causes dissociation into holo-complexes). In both detergents, we observed a strong reduction in the levels of complex I–containing supercomplex and complex I holoenzyme as detected with NDUFA9 or NDUFB6 antibodies (Fig. 2*A* and *B*, lanes 1–4). Complexes III and IV were not detected in the supercomplex in *SFXN4*^{KO} cells (Fig. 2*A*, lanes 7–10), and the holo-complex forms of these complexes were unaffected or, in the case of complex III, increased in abundance (Fig. 2*B*, lanes 7–10). The bioenergetic implication of this isolated complex I defect was evaluated

further using *SFXN4*^{KO} and *SFXN1*^{KO} cells (as control) (4). Enzymatic activity of the OXPHOS complexes was consistent with the BN-PAGE data, revealing a ~70% reduction in complex I activity in cells lacking *SFXN4* (Fig. 2*C*), while cells lacking *SFXN1* had no change in complex I activity (Fig. 2*C*). Consistent with their stability on BN-PAGE, the activities of complexes II, III, and IV were largely unaltered in *SFXN4*^{KO} cells (Fig. 2*C*). *SFXN4*^{KO} cells were also less capable of synthesizing ATP when provided with complex I substrates (glutamate + malate, pyruvate + malate) (Fig. 2*D*), while ATP production from complex II–driven respiration using succinate was unaffected. *SFXN4*^{KO} cells also exhibited reduced basal and maximal oxygen consumption rates (Fig. 2*E*) and possessed no glycolytic reserve (Fig. 2*F*), likely because the cells have adapted to rely on glycolysis for ATP production due to the strong complex I defect observed. Thus, cells lacking *SFXN4* display an isolated defect in complex I that perturbs mitochondrial respiration and ATP production.

A role for *SFXN4* in the biogenesis of iron-sulfur (Fe-S) clusters has been suggested (19). *SFXN*s 1, 2, and 3 are serine transporters (5), and it is plausible that *SFXN4* has functionally diverged to import cysteine, an amino acid that is structurally related to serine and which is required for Fe-S biogenesis (20). Although complex I contains Fe-S clusters and would be affected by a defect in Fe-S biogenesis, several Fe-S-containing proteins and complexes exist in mitochondria (including complexes II and III) that were unaffected by deletion of *SFXN4* (Fig. 1*C–E*). Additionally, supplementation of *SFXN4*^{KO} cells with supraphysiological concentrations of cysteine (as cystine or N-acetyl cysteine) was unable to rescue the complex I defect in *SFXN4*^{KO} cells (*SI Appendix, Fig. S1D*, lanes 4 and 5). These results suggest that *SFXN4* is required specifically for the assembly or stability of complex I.

***SFXN4* Interacts with the MCIA Complex.** We set out to determine the protein interaction network of *SFXN4* to determine how *SFXN4* may function in complex I biogenesis/assembly. *SFXN4*^{KO} HEK Flp-In cells were complemented with 1) untagged *SFXN4* or 2) ^{FLAG}*SFXN4*. *SFXN4* has previously been suggested to be a resident of the mitochondrial inner membrane (7). Indeed, *SFXN4* was present in the pellet fraction following carbonate extraction, suggesting that the protein is membrane integral (*SI Appendix, Fig. S2A*, lanes 14 and 16). Mitochondrial subfractionation showed both *SFXN4* (detected with a *SFXN4* polyclonal Ab raised against the N terminus) and ^{FLAG}*SFXN4* remain protected from protease in intact mitochondria (*SI Appendix, Fig. S2A*, lanes 1 and 2 and lanes 7 and 8) but become accessible to protease digestion following disruption of the outer membrane (*SI Appendix, Fig. S2A*, lanes 3 and 4 and lanes 9 and 10), suggesting the presence of the N terminus in the intermembrane space. We were unable to determine the topology of the C terminus, as various C-terminally tagged constructs expressed poorly and were unable to rescue the CI defect in the *SFXN4*^{KO} cells (*SI Appendix, Fig. S2B*), suggesting that they were not functional. We conclude *SFXN4* is localized to the inner membrane with its N terminus facing the intermembrane space. Based on a model where *SFXN* proteins have five transmembrane domains (5), its C terminus would face into the matrix.

The ^{FLAG}*SFXN4* construct was able to rescue the complex I defect in *SFXN4*^{KO} cells (Fig. 3*A*) and was used to identify interacting partners via affinity enrichment MS (AP-MS) (Fig. 3*B* and *C* and *SI Appendix, Table S2*). The three most enriched proteins were ECSIT, ACAD9, and NDUFAF1 (Fig. 3*B* and *C* and *SI Appendix, Table S2*), established assembly factors for

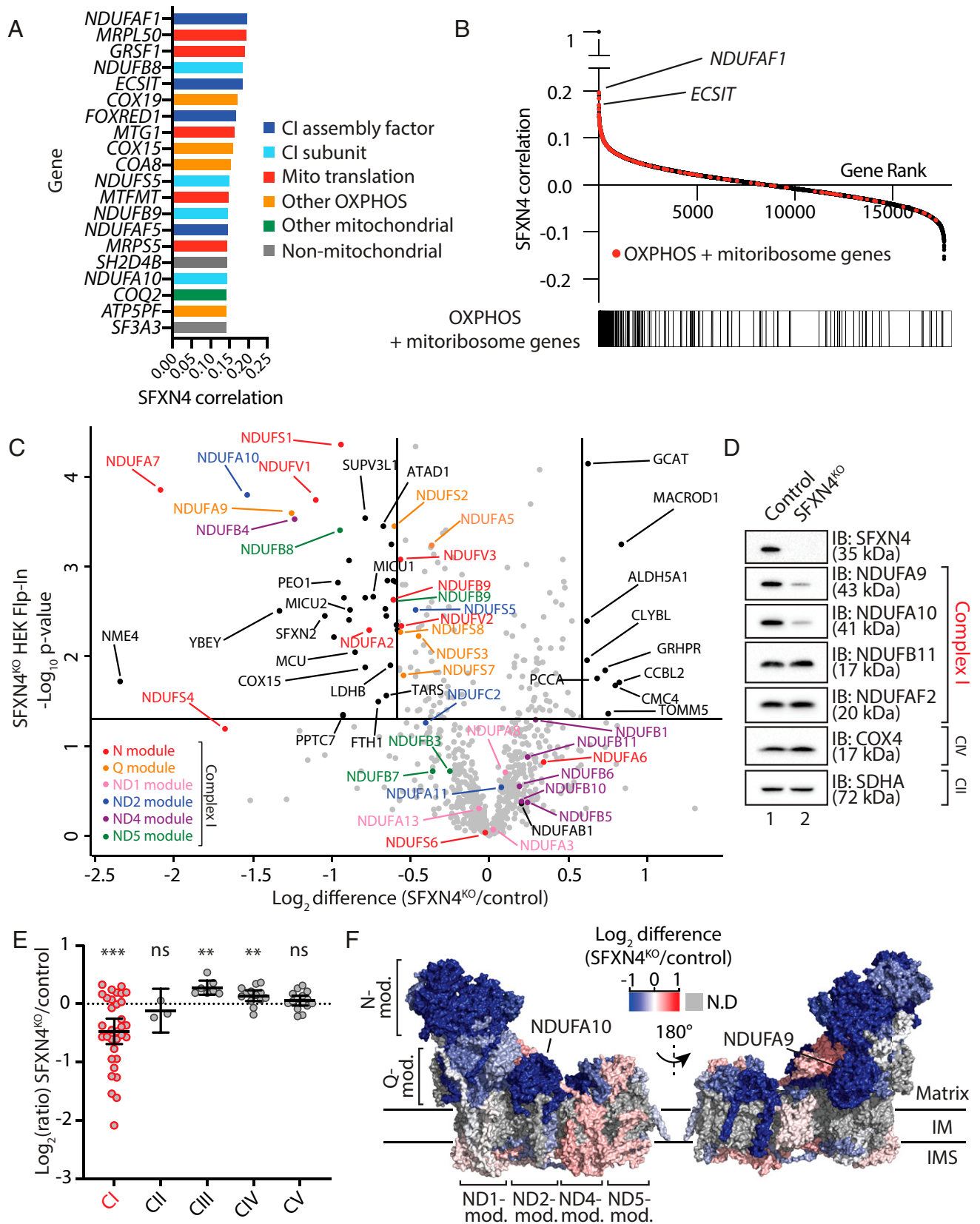


Fig. 1. SFXN4^{KO} leads to depletion of complex I subunits in mitochondria. (A) Top 20 most strongly correlated genes with SFXN4. Genes are ranked by Pearson correlation coefficient and color coded by functional category. (B) Genome-wide analysis of SFXN4 coessentiality. Genes are ranked according to correlation with SFXN4. Genes encoding proteins of the OXPHOS system and the mitoribosome are indicated in red on the graph and with black lines on the plot underneath. (C) Mitochondria from control and SFXN4^{KO} cells were subjected to label free quantitative MS analysis. The volcano plot depicts the levels of proteins in SFXN4^{KO} mitochondria relative to control ($n = 3$). Horizontal cutoff represents a P value of 0.05, and vertical cutoffs represent 1.5x fold change. Proteins are color coded according to the complex I assembly module to which they belong. (D) Mitochondrial lysates from control and SFXN4^{KO} HEK293 cells were analyzed by SDS-PAGE and immunoblotting. (E) Relative abundance of respiratory chain complexes (complexes I–V) in SFXN4^{KO} cells determined from data in (C) as compared to control. Mean \pm 95% CI is depicted. ** $P < 0.01$, *** $P < 0.001$, ns, not significant. (F) Topographical heatmap showing log₂ fold-change values for complex I subunits from SFXN4^{KO} mitochondria (PDB 5LDW).

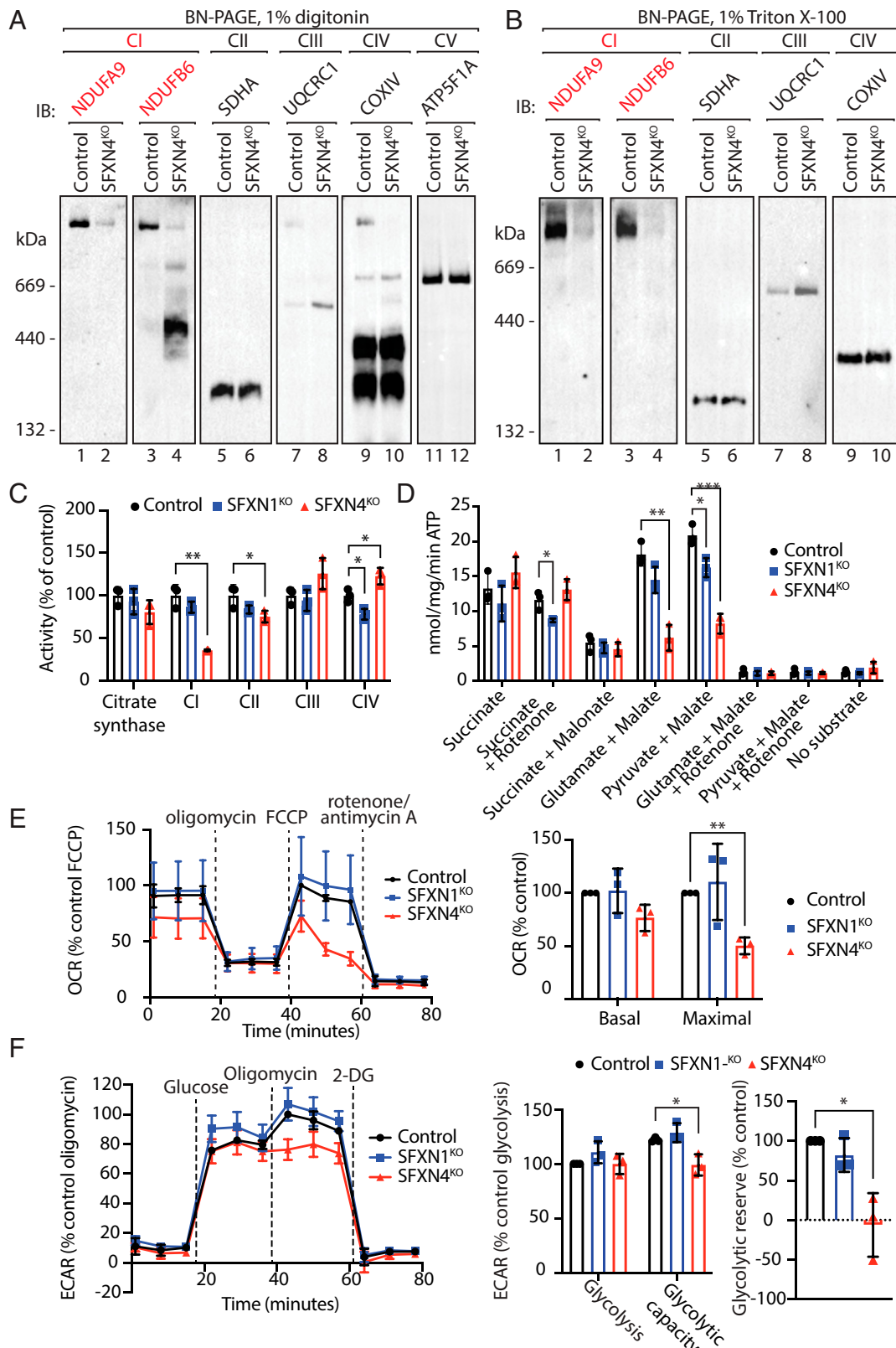


Fig. 2. SFXN4^{KO} leads to isolated complex I deficiency. (A and B) Mitochondria isolated from control and SFXN4^{KO} cells were solubilized in 1% digitonin- (A) or 1% Triton X-100- (B) containing buffer and analyzed by BN-PAGE and immunoblotting. (C) Spectrophotometric measurements of mitochondrial respiratory chain and citrate synthase enzyme activity in enriched mitochondrial fractions prepared from control, SFXN1^{KO}, and SFXN4^{KO} cells. Graph depicts mean \pm SD ($n = 3$). Two-sample t test: $*P < 0.05$, $**P < 0.01$. (D) Measurement of ATP synthesis rates in digitonin permeabilized cells provided with indicated CI (pyruvate, glutamate, malate), or CII (succinate) substrates or inhibitors (CI, rotenone; CII, malonate). Data are depicted as mean \pm SD ($n = 3$). Two-sample t test: $*P < 0.05$, $**P < 0.01$, $***P < 0.001$. (E) OCRs in live cells measured using a Seahorse analyzer to monitor mitochondrial stress following injections with indicated inhibitors (Left), with calculations of basal and maximal mitochondrial respiration (Right). One-sample t test (Right): $**P < 0.01$. (F) Glycolysis stress assay in live cells determined from extracellular acidification rates measured using a Seahorse analyzer following indicated injections (Left). Cellular glycolysis and maximal glycolytic capacity determined following glucose and oligomycin injections, respectively (Middle and Right). Data are depicted as mean \pm SD ($n = 3$). One sample t test (Middle and Right): $*P < 0.05$.

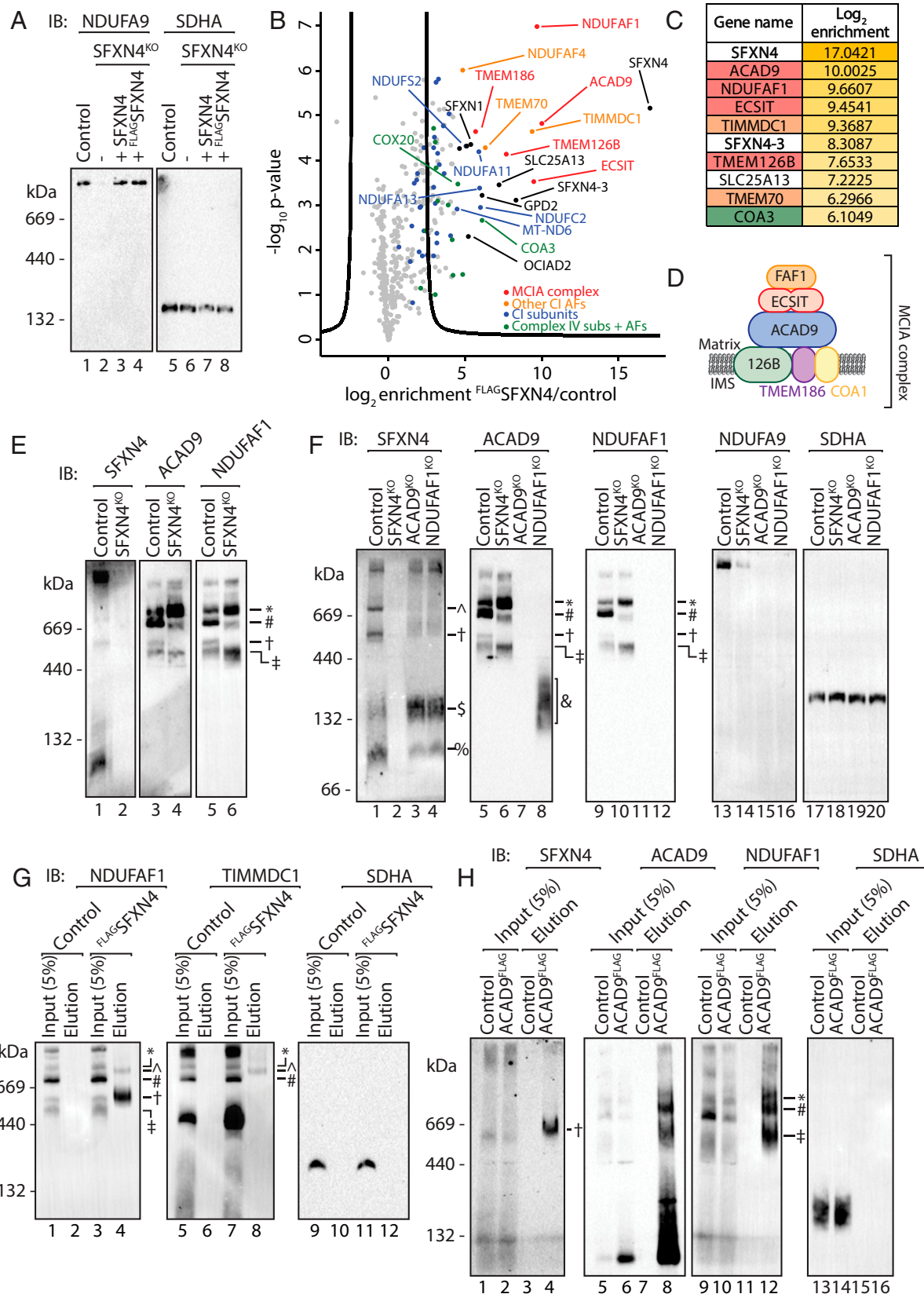


Fig. 3. SFXN4 interacts with the MCIA complex and is required for CI assembly. (A) Mitochondria isolated from control, SFXN4^{KO}, SFXN4^{KO} + SFXN4, and SFXN4^{KO} + FLAG-SFXN4 HEK293 cells were solubilized in 1% digitonin-containing buffer and analyzed by BN-PAGE and immunoblotting. (B) Anti-FLAG IP was performed using mitochondria isolated from control and SFXN4^{KO} + FLAG-SFXN4 HEK293 cells. Eluates were analyzed by LFQ proteomics, and significant interacting partners were visualized on a volcano plot. Curved line indicates significance determined using false discovery rate (FDR) statistics (FDR < 5%, S₀ = 12). Proteins are colored based on function. (C) Table depicting the 10 most strongly enriched proteins in the SFXN4^{KO} + FLAG-SFXN4 eluate relative to the control eluate. Gene names are color coded according to the legend in B. (D) Schematic depiction of the MCIA complex. (E and F) Mitochondria isolated from control and SFXN4^{KO} cells (E) or control, SFXN4^{KO}, ACAD9^{KO}, and NDUFAF1^{KO} cells (F) were solubilized in 1% digitonin and analyzed by BN-PAGE and immunoblotting. (G and H) Mitochondria isolated from control and SFXN4^{KO} + FLAG-SFXN4 cells (G) or control and ACAD9^{KO} + ACAD9^{FLAG} cells (H) were solubilized in 1% digitonin and subjected to anti-FLAG IP. Eluates were analyzed by BN-PAGE and immunoblotting.

complex I (11, 12). These genes exhibited a high degree of co-essentiality with *SFXN4* in the Achilles gene essentiality dataset analysis (Fig. 1A and *SI Appendix*, Fig. S3A), providing strong evidence that they represent functionally relevant interactions. Several other complex I subunits and assembly factors were also enriched in the eluate (Fig. 3B and C and *SI Appendix*, Table S2). Of note, another isoform of *SFXN4*, annotated as isoform 3, was identified in the AP-MS experiment (Fig. 3B and C and *SI Appendix*, Table S2). Unique peptides for isoform 3 are not present in the ^{FLAG}*SFXN4* construct; however, they could be encoded by *SFXN4* transcripts produced by alternate splicing and would thus not be deleted by the gRNA used to generate the *SFXN4*^{KO}. The protein encoded by isoform 3 lacks the first ~115 amino acids of *SFXN4* but still contains all 5 predicted transmembrane domains (*SI Appendix*, Fig. S3B). To confirm that the potential existence of *SFXN4* isoform 3 was not masking further defects, we generated additional HEK Flp-In *SFXN4*^{KO} cell lines (in the wild-type [WT] 293 Flp-InTM T-RexTM background) using a gRNA that would affect all predicted isoforms (*SI Appendix*, Fig. S3C). Proteomic analysis of mitochondria isolated from these cells by label-free quantitative MS revealed that they were largely indistinguishable from the original *SFXN4*^{KO} cells (*SI Appendix*, Fig. S3D and Table S3).

The most enriched interacting partners of *SFXN4* are components of the MCIA complex (Fig. 3D), a complex of assembly factors located at the mitochondrial inner membrane that mediates the assembly of the ND2 module of complex I (11, 12). Using BN-PAGE analysis, MCIA subunits can be detected across several different complexes that represent different complex I assembly intermediates (Fig. 3E, lanes 3 and 5) (10, 12, 13). The arrangement of MCIA complex containing complex I assembly intermediates was dramatically altered in *SFXN4*^{KO} cells (Fig. 3E, lanes 4 and 6), suggesting that steady-state intermediates containing the MCIA complex were perturbed. In particular, higher molecular weight intermediates (Fig. 3E, lanes 3–6, * and #), which are thought to contain at least the Q, ND1, and ND2 modules (the Q/P_p assembly intermediate) (12, 13), were altered substantially in the *SFXN4*^{KO} mitochondria. Specifically, the large high-molecular-weight intermediate (Fig. 3E, lanes 3 and 4, *) which is thought to contain the ND4 module but not the ND5 module (12) (a Q/P assembly intermediate lacking the ND5/P_D-b module; ref. 13), was accumulated in the *SFXN4*^{KO} mitochondria, while the smaller high-molecular-weight intermediate (Fig. 3E, lanes 3 and 4, #), which may represent the previously described 736-kDa Q/P_p intermediate, was dramatically reduced in abundance. These changes in distribution of the MCIA complex across different intermediates were not associated with changes to the abundance of MCIA complex proteins (*SI Appendix*, Fig. S4A, lanes 1 and 2) and could be reversed through complementation of the *SFXN4*^{KO} cell line with untagged *SFXN4* or ^{FLAG}*SFXN4* (*SI Appendix*, Fig. S4B).

Complexome profiling (11), a powerful MS-based proteomics technique for profiling the composition and size of protein complexes separated by BN-PAGE, was also used to analyze the changes to the MCIA complex in the *SFXN4*^{KO} cells (*SI Appendix*, Figs. S5A and S6 and Table S4). The complexome profiling data confirmed the observations made with Western blotting, revealing extensive rearrangements of MCIA complex intermediates (*SI Appendix*, Fig. S5A). Interestingly, a *SFXN4*-containing complex (Fig. 3E, lane 1, †) migrated similarly to a band detectable using ACAD9 or NDUFAF1 antibodies that was absent in *SFXN4*^{KO} cells (Fig. 3E, lanes 3–6, †). Although we were unable to detect *SFXN4* in this range in our own

complexome analysis (*SI Appendix*, Fig. S5A), we were able to identify a low-abundance population of *SFXN4* migrating alongside MCIA complex subunits in the complexome data from the published complexome profiling of WT and rho-0 cells, which lack mtDNA (*SI Appendix*, Fig. S5B) (21). Of note, these high-molecular-weight forms of *SFXN4* collapsed to lower molecular weight forms in rho-0 cells (*SI Appendix*, Fig. S5B).

If the *SFXN4*-containing complex observed by Western blot represented an interaction with the MCIA complex, we reasoned it should be absent in cell lines lacking core MCIA complex subunits. Indeed, higher molecular weight *SFXN4*-containing complexes were destabilized in ACAD9^{KO} or NDUFAF1^{KO} cell lines (Fig. 3F, lanes 3–4, ^ and †; *SI Appendix*, Fig. S4C). Further confirmation that this complex represents an interaction between *SFXN4* and the MCIA complex was obtained by performing ^{FLAG}*SFXN4* immunoprecipitations (IPs) and analyzing eluate fractions by BN-PAGE and immunoblotting with antibodies for MCIA subunits (Fig. 3G). *SFXN4* enriched NDUFAF1 in a complex comigrating with the above-described putative *SFXN4*-MCIA complex (Fig. 3G, lane 4, †), as well as a higher complex (Fig. 3G, lane 4, ^). TIMMDC1, an assembly factor responsible for assembly of the ND1 module of complex I (12, 13), could be detected only in the upper species (Fig. 3G, lane 8, ^), suggesting that this complex (^) represents a further progressed complex I intermediate containing both the ND2 and the ND1 modules (13). To confirm that the lower *SFXN4* complex (†) contained a pool of the entire MCIA complex, we repeated the experiment and immunoblotted for both NDUFAF1 and ACAD9 (*SI Appendix*, Fig. S4D). Indeed, both proteins could be detected in the complex (*SI Appendix*, Fig. S4D, lanes 4 and 8, †), and the interactions were confirmed via SDS-PAGE (*SI Appendix*, Fig. S4E, lane 5). We confirmed that the observed association between *SFXN4* and the MCIA complex was not an artifact of ^{FLAG}*SFXN4* overexpression by performing a reciprocal IP experiment using an ACAD9^{FLAG} cell line (Fig. 3H). The ACAD9^{FLAG} IP eluate contained an endogenous *SFXN4* complex at the expected size (Fig. 3H, lane 4, †), confirming the existence of the *SFXN4*-MCIA complex. The interaction between endogenous *SFXN4* and ACAD9^{FLAG} could also be detected via SDS-PAGE (*SI Appendix*, Fig. S4F, lane 5). Together, these results demonstrate that *SFXN4* associates with an MCIA complex-containing assembly intermediate and likely functions as a complex I assembly factor.

SFXN4 Is Required for Incorporation of MT-ND6 into the ND2 Module. The complex that contains *SFXN4* and the MCIA complex (Fig. 3F, lane 1, †) migrates just above the core MCIA-ND2 module complex (Fig. 3F, lanes 5 and 9, ‡), suggesting that *SFXN4* acts in complex I assembly after the formation of the core MCIA-ND2 module. Complexome and biochemical studies suggest that ND6 is the last subunit to be added to the ND2 module during its assembly (13, 22) and that ND6 incorporation occurs in a distinct step. It seems plausible that the *SFXN4*-containing MCIA complex (†) represents *SFXN4*-MCIA bound to the completed ND2 module, and the function of *SFXN4* is to deliver ND6 into this complex. This hypothesis is supported by the observation that ND6 was the most enriched mtDNA-encoded protein detected in the FLAG-*SFXN4* IP MS (Fig. 3B and *SI Appendix*, Table S2).

We investigated the steady-state levels of ND6 in cells lacking *SFXN4* using SDS-PAGE and immunoblotting. Consistent with a potential requirement of *SFXN4* for its biogenesis, ND6

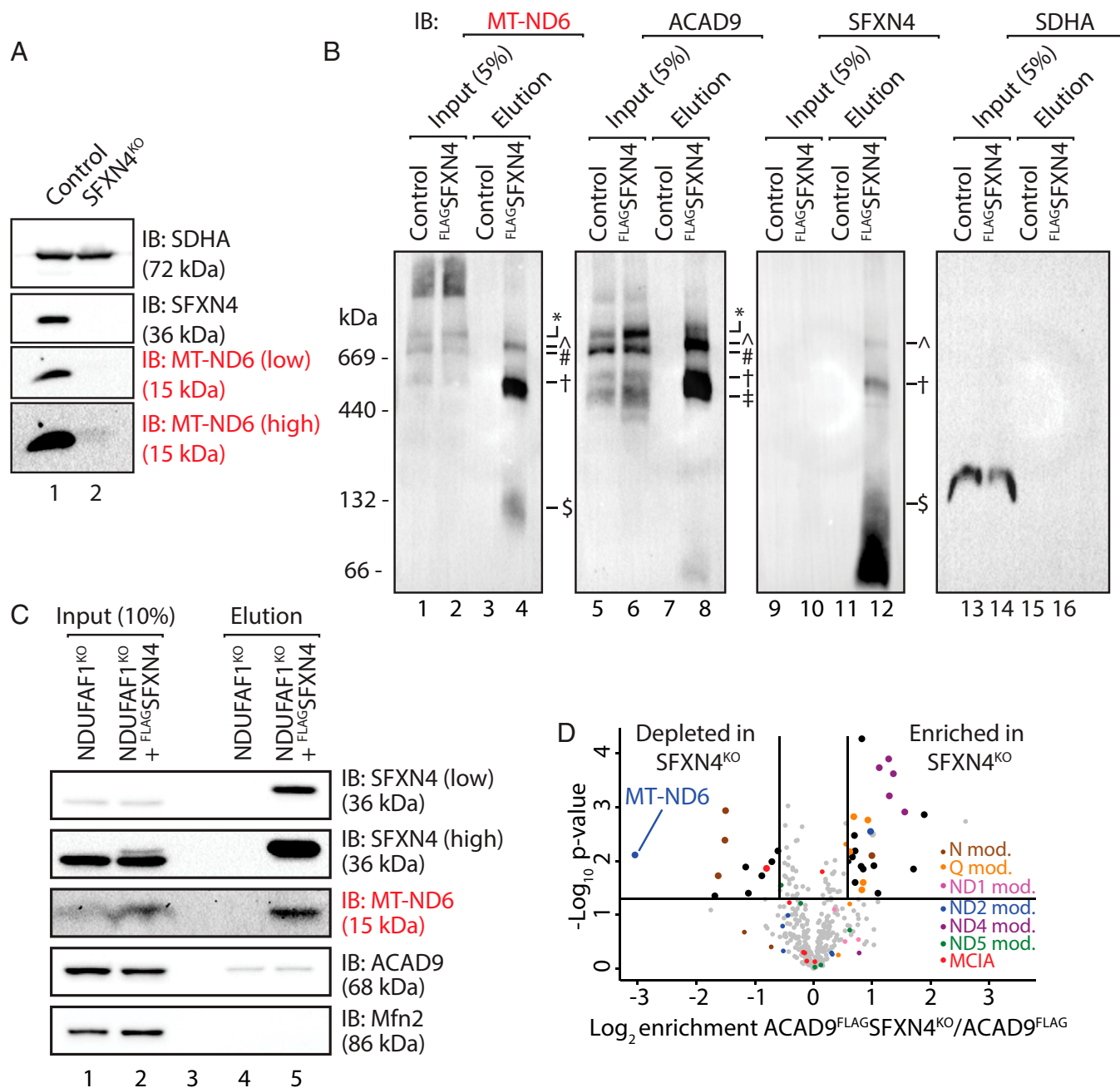


Fig. 4. SFXN4 mediates the incorporation of MT-ND6 into complex I. (A) Mitochondrial lysates from control and SFXN4^{KO} cells were analyzed by SDS-PAGE and immunoblotting. (B) Mitochondria isolated from control and SFXN4^{KO} + FLAG-SFXN4 cells were solubilized in 1% digitonin and subjected to anti-FLAG IP. Eluates were analyzed by BN-PAGE and immunoblotting. (C) Mitochondria isolated from NDUFAF1^{KO} and NDUFAF1^{KO} + FLAG-SFXN4 cells were solubilized in 1% digitonin and subjected to anti-FLAG IP. Eluates were analyzed by SDS-PAGE and immunoblotting. (D) Anti-FLAG IP was performed using mitochondria isolated from control (ACAD9^{KO} + ACAD9^{FLAG}) and ACAD9 + ACAD9^{FLAG} SFXN4^{KO} cells. Eluates were analyzed by label-free quantitative MS. The volcano plot depicts the levels of ACAD9-interacting partners in SFXN4^{KO} cells relative to control cells ($n = 3$). Proteins on the right of the volcano were more abundant in the ACAD9^{FLAG} IP from the SFXN4^{KO} cell line, and proteins on the left of the volcano were more abundant in the ACAD9^{FLAG} precipitation from the control cell line. Horizontal cutoff represents a P value of 0.05, and vertical cutoffs represent 1.5x fold change. Proteins are color coded according to the complex I assembly module to which they belong.

was barely detectable in mitochondria isolated from SFXN4^{KO} cells (Fig. 4A). To investigate the potential interaction between SFXN4 and ND6, we performed FLAG-SFXN4 IP and analyzed the eluate by BN-PAGE and Western blotting with the ND6 antibody. ND6 was easily detectable in the main SFXN4-MCIA complex (Fig. 4B, lanes 4, 8, and 12, †), suggesting that this complex does, indeed, represent the complete ND2 module. ND6 was detectable in a smaller ~132-kDa complex by BN-PAGE (Fig. 4B, lane 4, \$) that was reminiscent of a low-molecular-weight SFXN4-containing complex that we had

observed across other experiments (Fig. 3F, lanes 1–4, \$). Notably, the 132-kDa SFXN4-containing complex, as well as higher SFXN4-containing complexes, are sensitive to treatment with chloramphenicol (CAP), a mitochondrial translation inhibitor (SI Appendix, Fig. S7A, lanes 1–5, \$ and †), and recovered progressively in a 24-h period after removal of CAP (4–8 h for the 132-kDa complex [\$], 4–24 h for the SFXN4-MCIA complex [†]) (SI Appendix, Fig. S7B, lanes 1–7, \$ and †), suggesting that formation of these complexes is dependent on the presence of an mtDNA-encoded protein. We detected no MCIA subunits

in the 132-kDa complex in ^{FLAG}SFXN4 IP BN-PAGE experiments (Fig. 3G, lane 4; *SI Appendix*, Fig. S4D, lanes 4 and 8). This complex could represent an interaction between SFXN4 and ND6 that facilitates the subsequent incorporation of ND6 into the nearly complete ND2 module, but this requires further experimental validation.

To investigate whether a direct interaction between SFXN4 and ND6 could be detected, we performed ^{FLAG}SFXN4 IP experiments at various timepoints following a 2-d CAP treatment (*SI Appendix*, Fig. S8A), which allowed for turnover of most complex I assembly intermediates (*SI Appendix*, Fig. S7A). Analysis of eluates by SDS-PAGE (*SI Appendix*, Fig. S8B) demonstrated that the interaction between SFXN4 and ND6 was re-established rapidly at early timepoints (*SI Appendix*, Fig. S8B, lanes 7–12). This was also the case for interactions between SFXN4 and MCIA complex subunits (*SI Appendix*, Fig. S8B, lanes 7–12), making it difficult to determine whether the interaction between SFXN4 and ND6 is direct. Analysis of eluates by BN-PAGE (*SI Appendix*, Fig. S8C) demonstrated that the ~132-kDa ND6-containing complex (*SI Appendix*, Fig. S8C, §) and the SFXN4-MCIA-ND6 complex (*SI Appendix*, Fig. S8C, †) increased steadily in abundance and largely in parallel following CAP removal (*SI Appendix*, Fig. S8C, lanes 6–10). To provide further insight into the interaction between SFXN4 and ND6, we expressed ^{FLAG}SFXN4 in a cell line lacking NDUFAF1. As demonstrated in Fig. 3F and by Formosa and colleagues (12), the MCIA complex is destabilized in the absence of NDUFAF1, and the preservation of an interaction between SFXN4 and ND6 in this cell line would indicate that the interaction can occur independently of an assembled MCIA complex. Indeed, the SFXN4-ND6 interaction was captured following ^{FLAG}SFXN4 IP from mitochondria isolated from the NDUFAF1^{KO} cell line (Fig. 4C). This provides strong support for a direct interaction between SFXN4 and ND6 independent of MCIA. The ~132-kDa complex observed on BN-PAGE could represent this interaction, but further work is required to confirm whether this is the case and whether it forms prior to the interaction between SFXN4 and the MCIA complex.

To further understand the contribution of SFXN4 to complex I assembly, we sought to quantitatively determine the changes in composition and abundance of MCIA complex I assembly intermediates following SFXN4 deletion. We generated a SFXN4^{KO} cell line in the background of an ACAD9^{KO} cell line stably re-expressing ACAD9^{FLAG} and performed ACAD9^{FLAG} IPs (*SI Appendix*, Fig. S9A). The ACAD9^{FLAG}/SFXN4^{KO} cell line showed the same MCIA complex rearrangements and complex I disruption as SFXN4^{KO} cells by BN-PAGE and SDS-PAGE (*SI Appendix*, Fig. S9B and C). IPs of ACAD9^{FLAG} in the absence of SFXN4 significantly enriched subunits from the ND4 module, as well as the ND4 module assembly factor TMEM70 (*SI Appendix*, Fig. S9D and Table S5), suggesting that the accumulated intermediate observed in the SFXN4^{KO} cells (*SI Appendix*, Fig. S9B, lanes 8–9 and 11–12, *, and Fig. 3E, lanes 3–6, *) contains the ND4 module. The ND1 and Q modules were also enriched, albeit to lesser extents, suggesting that this stalled intermediate might contain the Q, ND1, ND2, and ND4 modules (Q/P_p/P_p-a). Strikingly, ND6 was significantly reduced in the ACAD9^{FLAG} IPs from the SFXN4^{KO} cells compared to control ACAD9^{FLAG} cells containing SFXN4 (Fig. 4D and *SI Appendix*, Fig. S9D and Table S5), providing further evidence that SFXN4 is required for the delivery of ND6. Importantly, other subunits of the ND2 module, including ND2, ND3, NDUFC2, and NDUFA10, were not depleted or enriched in complexes from

the SFXN4^{KO} cells (Fig. 4D and *SI Appendix*, Fig. S9D and Table S5), suggesting that other subunits of the ND2 module can still be incorporated into complex I assembly intermediates in the absence of SFXN4.

Taken together, our data suggest that SFXN4 is a complex I assembly factor that is required for the efficient incorporation of ND6 into complex I through an association with the MCIA complex.

Discussion

This study demonstrates that the mitochondrial disease-linked protein SFXN4, a member of the recently characterized SFXN family, functions as a complex I assembly factor. SFXN4^{KO} cells display reduced steady-state levels of complex I subunits, resulting in the loss of respiratory supercomplexes, significant reductions in complex I activity, and impaired mitochondrial respiration. The severity of this isolated complex I phenotype aligns with SFXN4 being the only SFXN currently implicated in clinical cases of mitochondrial disease (7, 8).

Our results show that SFXN4 interacts with the MCIA complex, a network of assembly factors required for assembly of the ND2 module (11). The ND2 module contains four subunits encoded by the mitochondrial genome: ND2, ND3, ND4L, and ND6. Multiple studies have shown that ND2 and the MCIA complex appear to assemble initially, before ND3, ND4L, and ND6 are added sequentially (13, 22). The MCIA complex comprises six proteins (ACAD9, NDUFAF1, ECSIT, TMEM126B, TMEM186, and COA1) with varying degrees of interdependence. Subunits of core MCIA complex—particularly, NDUFAF1, ACAD9, ECSIT, and COA1—are crucial for incorporation of ND2 (12, 23), and TMEM186 was recently proposed to play a specific role in the incorporation of ND3 (12). Currently, no specific assembly factor(s) have been described for ND4L or ND6, which are the two last subunits added to the ND2 module (13, 22). Our results suggest that SFXN4 is required for the correct incorporation of ND6 into the ND2 module at the final steps of its assembly and that the loss of this activity leads to impaired complex I assembly and isolated complex I deficiency. This is based on several pieces of evidence: 1) MT-ND6 was the most significantly enriched mtDNA-encoded protein immunoprecipitated with ^{FLAG}SFXN4; 2) ND6 and SFXN4 associate with the MCIA complex simultaneously, suggesting that SFXN4 is involved in the recruitment of ND6; 3) stalled complex I assembly intermediates in SFXN4^{KO} cells lack MT-ND6, suggesting that preceding steps in MCIA complex and ND2 module assembly are unaffected; and 4) SFXN4 and ND6 can still interact independently of the MCIA complex. The exact molecular role of SFXN4 in the biogenesis/assembly of ND6 remains to be determined. ND6 could be expressed and rapidly degraded in SFXN4^{KO} cells due to an inability to progress further in its assembly pathway in the absence of SFXN4. Alternatively, another model worth considering is that SFXN4 plays a role in promoting the translation of ND6, perhaps in a similar manner to how COA1 is involved in the translation of ND2 (23). Either scenario represents an exciting avenue of future research.

The function for SFXN4 as a complex I assembly factor provides an explanation for the disease phenotype caused by mutations in *SFXN4* (7, 8). Currently, three patients have been described, and all presented with severe complex I deficiency, lactic acidosis, visual impairment, and microcephaly, while two of the three patients presented with macrocytic anemia. Previous studies have suggested that SFXN4 functions in the

biogenesis of Fe-S clusters (19), which are present in multiple complex I subunits and could therefore explain the complex I deficiency observed in patients with *SFXN4* mutation. Based on this, it would be expected that *SFXN4* would function in the transport of iron or cysteine, the two components of Fe-S clusters. However, mitochondrial iron transporters (SLC25A28 and SLC25A37) have already been identified (24), and it seems more reasonable to suggest that *SFXN1* and *SFXN3* represent at least part of the mitochondrial cysteine import machinery based on the ability of cysteine to compete with serine for transport by *SFXN1* (5). We showed that supplementation with excess cysteine was not able to rescue the complex I defect in our system, and we observed no impact on other respiratory complexes that also contain Fe-S cluster proteins. Dysfunction of complex I has been shown to result in impairment of Fe-S cluster biosynthesis (25), so it is possible that observations of reduced Fe-S cluster biosynthesis in *SFXN4*^{KO} cells represent a secondary effect occurring downstream of complex I dysfunction. Our study highlights the importance of leveraging multiple unbiased approaches, including gene coessentiality analysis, cell/organelle proteomics, and IP MS, when seeking insights into specific molecular functions of proteins mutated in disease.

SFXNs represent a family of mitochondrial proteins that, until recently, remained poorly characterized. *SFXNs* 1 and 3 (and, potentially, 2) have been identified as amino acid transporters, and it seemed likely that other members of the gene family would perform a similar function, albeit for different molecules. Of the five *SFXNs*, *SFXN1/2/3* are closely related, with *SFXN1* and *SFXN3* sharing 76% sequence identity and *SFXN2* having 55% sequence identity with both *SFXN1* and *SFXN3*. *SFXN4* and *SFXN5* appear phylogenetically distinct from the other members, with *SFXN4* the more divergent of the two (*SI Appendix, Fig. S10A*). Our results lead to the conclusion that *SFXN4* has indeed diverged evolutionarily to perform a role as an assembly factor for complex I. Such a shift in function is not unprecedented; for example, the proteins TIMMDC1 (26, 27) and NDUFA11, which function as an assembly factor and a subunit for complex I, respectively, are evolutionarily related to the Tim17/Tim22/Tim23 family of mitochondrial import proteins (28). It is important to note that *SFXN4* is not absolutely required for complex I biogenesis, as some complex I is able to assemble in its absence, and patients with homozygous loss-of-function mutations in *SFXN4* are able to live into at least early adolescence (7, 8). It will be interesting to determine when *SFXN4* emerged as a complex I assembly factor from an evolutionary perspective and whether its role is conserved in some lineages and lost in others, as a recent study demonstrated has occurred for *COA1* (29).

Methods

CERES Gene Essentiality Analysis. For gene dependency analysis, gene effect data were extracted from <http://www.depmap.org> (17, 18) (Accessed: 15th July 2021). CRISPR dataset: DepMap 21Q2 Public+Score, CERES). Pearson correlations between genetic dependency on *SFXN1*, *SFXN2*, *SFXN4*, *SFXN4*, *SFXN5*, and all other genes were computed using the `cor.test` function in R (Version 3.6.0) across 989 cell lines and ~18,000 genes. Genes were ranked by Pearson correlation coefficients.

Cell Lines, Cell Culture, and Stable Cell Line Generation. All cell lines were cultured in Dulbecco's Modified Eagle Medium (DMEM) (Thermo Fisher Scientific) containing 1% (vol/vol) penicillin-streptomycin (Thermo Fisher Scientific) and supplemented with 5% (vol/vol) fetal bovine serum (Sigma-Aldrich). Cells were cultured at 37°C in a humidified atmosphere containing 5% CO₂. For chloramphenicol treatment and chase experiments, cells were cultured for 1–4 d in DMEM supplemented with 50 µg/mL uridine (Sigma-Aldrich) and 50 µg/mL

CAP (Sigma-Aldrich) to inhibit the mitochondrial ribosome and deplete OXPHOS complexes. For the chase experiments, the CAP-containing media were removed after a 2-d treatment, and cells were washed twice with phosphate buffered saline (PBS). Regular culture media supplemented with 50 µg/mL uridine were then added to permit reinitiation of mitochondrial translation, and cells were harvested for mitochondrial isolation at the desired timepoints.

Stable tetracycline-inducible Flp-InTM T-RexTM HEK293 cell lines were generated using the T-RexTM Flp-InTM system (Thermo Fisher Scientific) as previously described (30). Briefly, Flp-InTM T-RexTM 293 cells were cotransfected with pOG44 (encoding the Flp recombinase) and a pcDNA5/FRT/TO plasmid (containing the open reading frame of the gene of interest) at a 9:1 ratio, using Lipofectamine 3000 (Thermo Fisher Scientific) according to the manufacturer's instructions. Selection of positive clones commenced 72 h after the transfection using culture media supplemented with 200 µg/mL Hygromycin B (Thermo Fisher Scientific). Individual foci were expanded once visible and were screened for tetracycline-inducible expression of the protein of interest by culturing the cells overnight in culture media supplemented with 1 µg/mL tetracycline.

Stable tetracycline-inducible HEK293 NDUFAF1^{KO} + FLAG⁺*SFXN4* cell lines were generated using the Lenti-X Tet-On Inducible Expression System (Takara Bio). Briefly, HEK293 cells were transfected with pLVX-TetOn-FLAG-*SFXN4*-puro and lentiviral packaging vectors (pVSV-G and pSPAX2) using Lipofectamine 3000. Viral supernatant was harvested at 48 h post-transfection and layered onto target cells in the presence of 8 µg/mL polybrene. The transduced cells were selected using 1 µg/mL puromycin.

SFXN1^{KO}, *NDUFAF1*^{KO}, *ACAD9*^{KO}, and *ACAD9*^{KO} + *ACAD9*^{FLAG} cell lines were generated and characterized previously (4, 12).

Gene Editing and Screening. Editing of the *SFXN4* gene was carried out using the pSpCas9(BB)-2A-GFP CRISPR Cas9 construct (a gift from F. Zhang; Massachusetts Institute of Technology, Cambridge, MA; Addgene). CRISPR-Cas9 guide RNAs targeting exon 1 or exon 8 of the *SFXN4* gene were designed using CHOP-CHOP (31). Oligonucleotide duplexes (5'-CACCGGTGATCCAGAAGCGCACGT-3' and 5'-AAACACGTGCGCTCTGGATCACCC-3' for exon 1; 5'-CACCGCTGTGAACGCTGCCATGT-3' and 5'-AAACACATGGCAGCGTCAACAGCC-3' for exon 8) were ligated into pSpCas9(BB)-2A-GFP CRISPR-Cas9 and transfected into Flp-InTM T-RexTM 293 cells using Lipofectamine 3000. Single cells were obtained and deposited 24 h after transfection into a 96-well plate using fluorescence-activated cell sorting based on green fluorescent protein (GFP) fluorescence. Sorted cells were allowed to expand and screened by Western blotting using a *SFXN4*-specific antibody. Selected clones were verified through Sanger sequencing of the targeted site in the *SFXN4* gene.

Mitochondrial Isolation, Mitochondrial Subfractionation, Gel Electrophoresis, and Immunoblot Analysis. Mitochondria were isolated from cultured cells using a differential centrifugation protocol exactly as described previously (4). For experiments where whole cell samples were analyzed, cell pellets were resuspended in 1× lysis buffer (150 mM NaCl, 1% [vol/vol] Triton X-100, 0.1% [wt/vol] SDS, 10 mM Tris, pH 7.45, 5 mM EDTA) and incubated on ice for 30 min. Lysates were centrifuged at 16,000 × *g* and 4°C for 20 min to remove insoluble material, and protein concentration in the clarified supernatant was determined using the Pierce BCA protein assay kit.

For mitochondrial subfractionation experiments, 50 µg pellets of mitochondria were resuspended at 1 mg/mL in either isolation buffer (20 mM HEPES-KOH, pH 7.6, 220 mM mannitol, 70 mM sucrose, 1 mM EDTA, 0.5 mM phenylmethylsulfonyl fluoride [PMSF], and 2 mg/mL bovine serum albumin), swelling buffer (10 mM Hepes, pH 7.4), or 0.5% Triton X-100. Two samples were set up for each buffer; one was left untreated, and the other was treated consecutively with proteinase K (50 µg/mL for 10 min on ice) and PMSF (1 mM for 5 min on ice), before being precipitated with trichloroacetic acid (TCA). For carbonate extraction experiments, 100 µg mitochondrial pellets were resuspended in freshly prepared 100 mM Na₂CO₃ (pH 11.5) and incubated on ice for 30 min. Centrifugation at 100,000 × *g* and 4°C for 30 min was performed to separate membrane (pellet) and soluble (supernatant) fractions, which were both TCA precipitated. TCA precipitation was performed through the addition of 72% [wt/vol] TCA to a final concentration of 12.5%. Samples were mixed thoroughly and were incubated on ice for 30 min or overnight at –20°C. After centrifuging at 16,000 × *g* to pellet the precipitated material, pellets were washed with ice cold 70% acetone and allowed to air-dry.

Tris-tricine SDS-PAGE was carried out exactly as described previously (4, 32). In total, 10–16% acrylamide gradient gels were created using a gradient mixer. Samples for analysis were resuspended directly in SDS-loading dye (50 mM Tris-Cl, pH 6.8, 100 mM dithiothreitol [DTT], 2% [wt/vol] SDS, 10% [vol/vol] glycerol, 0.1% [wt/vol] bromophenol blue), or were combined with a 4× stock of the SDS-loading dye to a final concentration of 1×. Samples were boiled in the loading dye at 95°C for 5 min prior to loading. For experiments where mtDNA-encoded proteins were analyzed, samples were heated at only 50°C to avoid aggregation induced by excessive heat. Electrophoresis was generally performed overnight using Tris-tricine SDS-PAGE cathode buffer (0.1 M Tris, 0.1 M tricine, 0.1% [wt/vol] SDS, pH 8.45) and anode buffer (0.2 M Tris, pH 8.9).

BN PAGE was carried out exactly as described previously (4). Depending on the experiment, 4–13% or 4–16% acrylamide gradient gels were used. Preparation of samples for BN-PAGE analysis varied depending on the experiment. For isolated mitochondria, samples were resuspended at 1 mg/mL in digitonin-containing solubilization buffer (20 mM Bis-Tris, 50 mM NaCl, 10% [vol/vol] glycerol, pH 7.4, 1% [wt/vol] digitonin). Solubilization was allowed to occur on ice for 30 min, before insoluble material was removed through centrifugation at 16,000 × *g* for 30 min. BN loading dye (0.5% [wt/vol] Coomassie blue G250, 50 mM ϵ -amino *n*-caproic acid, 10 mM Bis-Tris, pH 7.0) was added to the clarified supernatant prior to loading. For IP eluates, BN loading dye was added directly to the eluate, which was immediately loaded. Electrophoresis was performed overnight at 4°C with BN anode buffer (50 mM Bis-Tris, pH 7.0) and cathode buffer (50 mM tricine, 15 mM Bis-Tris, 0.02% [wt/vol] Coomassie blue G250). After ~2 h of electrophoresis, the “blue” cathode was swapped for “clear” BN cathode, which lacks the Coomassie blue G250.

Following electrophoresis, semidry western transfer was performed using the Owl HEP-1 Semidry Electroblothing system (Thermo Fisher Scientific). Gels were transferred onto 0.45 μ M polyvinylidene fluoride membranes (0.45 μ M Immobilon-P; Merck). Following blocking for 1 h in PBS containing 5% [wt/vol] skim milk powder, membranes were incubated with specific primary antibodies. Primary antibodies used in the study were as follows: anti-ACAD9 (in-house, Ryan Laboratory), anti-ATP5F1A (Abcam; ab14748), anti- β -actin (Sigma-Aldrich; A2228), anti-COX4 (Cell Signaling Technology; 4850), anti-FLAG (Sigma-Aldrich; F1804), anti-HA (BioLegend), anti-Mfn2 (in house, Ryan Laboratory), anti-Myc (Abcam; ab9106), anti-MT-ND6 (Thermo Fisher Scientific; PA5-109993), anti-NDUFA10 (Santa Cruz Biotechnology; sc-376357), anti-NDUFA9 (in house, Ryan Laboratory), anti-NDUFAF1 (in house, Ryan Laboratory), anti-NDUFAF2 (in house, Ryan Laboratory), anti-NDUFB11 (Santa Cruz Biotechnology; sc-393110), anti-NDUFB6 (in house; Ryan Laboratory), anti-NDUFV2 (Proteintech; 15301-1-AP), anti-OPA1 (BD Biosciences; 612606), anti-SDHA (Abcam; ab14715), anti-SFXN4 (Cusabio; CSB-PA744046LA01HU), anti-TIMMDC1 (Sigma-Aldrich; HPA053214), and anti-UQCRC1 (Abcam; ab110252). After incubation overnight at 4°C or for several hours at room temperature, membranes were washed with PBS and incubated with anti-Mouse or anti-Rabbit horseradish peroxidase coupled secondary antibodies (Sigma-Aldrich) at a 1:10,000 dilution. Imaging was performed on a Chemi-Doc XRS+ imaging machine (BioRad) using Clarity Western ECL Substrate (BioRad).

Immunoprecipitation. IP of FLAG-tagged proteins was performed for downstream analysis by MS, SDS-PAGE, and BN-PAGE. For MS experiments, ~1 mg mitochondria was analyzed per replicate. For SDS-PAGE and BN-PAGE experiments, 300 μ g and 500 μ g mitochondria were analyzed, respectively. For IP experiments, mitochondria isolated from control cells and from cells expressing the FLAG-tagged protein of interest were resuspended at 2 mg/mL in 1% digitonin-containing solubilization buffer and incubated on a rotary wheel at 4°C for 40 min. Lysates were centrifuged at 16,000 × *g* and 4°C for 20 min to remove insoluble debris, and clarified supernatants were transferred to tubes containing FLAG affinity gel (Sigma-Aldrich) that had been pre-equilibrated in wash buffer (20 mM Bis-Tris, 50 mM NaCl, 10% [vol/vol] glycerol, pH 7.4, 0.1% [wt/vol] digitonin). For experiments analyzed by SDS or BN PAGE, 10% of the clarified supernatant was removed for analysis as a total fraction. For MS experiments, the clarified lysate was diluted with dilution buffer (20 mM Bis-Tris, 50 mM NaCl, 10% [vol/vol] glycerol, pH 7.4) to a digitonin concentration of 0.1% prior to the addition of the FLAG affinity gel. Clarified lysates were incubated with the FLAG affinity gel for 1 h on a rotary wheel at 4°C, after which the supernatant (containing unbound proteins) was removed, and the affinity gel

was washed three to four times with wash buffer. Subsequent processing varied depending on whether the elutions were analyzed by MS or PAGE. For samples intended for MS, elution of bound proteins was achieved through incubation of the resin with a low-pH elution buffer (0.2 M glycine, pH 2.5). Two 100- μ L elutions were performed, which were subsequently combined and precipitated through the addition of 1 mL cold 100% acetone. For samples intended for BN-PAGE and SDS-PAGE analysis, elution was achieved using 150 μ g/mL FLAG peptide in solubilization buffer containing 0.1% [wt/vol] digitonin. BN loading dye was added to samples for BN-PAGE, while samples for SDS-PAGE were TCA precipitated. TCA precipitation was not performed in experiments where mtDNA-encoded proteins were analyzed. In these experiments, SDS-PAGE loading dye was added directly to the total and elution fractions, which were boiled at 50°C for 5 min prior to loading.

Respiratory Chain Enzymology. Respiratory chain enzyme activities were measured by spectrophotometry as described (33), using enriched mitochondrial fractions with (CI, CII, CIV, and CS) or without (CIII) hypotonic treatment prepared from Flp-InTM T-RexTM 293 cells grown in triplicate flasks under standard conditions. CI was measured as rotenone-sensitive NADH:CoQ₁ oxidoreductase, measuring NADH oxidation at 340 nm. CII activity was measured as succinate:CoQ₁ oxidoreductase, measuring CoQ₁ reduction at 280 nm. CIII was assayed as decylbenzylquinol: cytochrome *c* reductase, measuring cytochrome *c* reduction at 550 nm. CIV was measured as cytochrome *c* oxidase, monitoring cytochrome *c* oxidation at 550 nm. The citrate synthase catalyzed production of coenzyme A (CoA:SH) from oxaloacetate was assayed by monitoring the formation of 5-thio-2-nitrobenzoate anions at 412 nm resulting from the spontaneous reaction of free sulfhydryl groups with the thiol reagent 5,5'-dithio-bis-(2-nitrobenzoic acid). Enzyme activities were calculated as initial rates (complexes I, II, and citrate synthase) or as first-order rate constants (complexes III and IV) (33).

Cellular Respiration and Glycolysis Measurements. Oxygen consumption rates (OCRs) and extracellular acidification rates (ECARs) were measured in live cells using a Seahorse Bioscience XF24-3 Analyzer according to manufacturer's procedures. Briefly, 50,000 cells were plated per well in XF24-3 culture plates treated with poly-D-lysine and grown overnight under standard culture conditions. For each cell line, six or seven replicate wells were measured in multiple plates (*n* = 3) with three measurement cycles of 2-min mix, 2-min wait, and 3-min measure. For mitochondrial stress assays, cells were assayed in nonbuffered Seahorse DMEM base medium (Agilent 102353-100) containing 25 mM glucose, 1 mM sodium pyruvate, and 2 mM glutamine using sequential injections of 0.5 μ M oligomycin, 0.1 μ M carbonyl cyanide 4-(trifluoromethoxy) phenylhydrazone (FCCP), and 0.5 μ M rotenone/0.3 μ M antimycin A. For glycolysis stress assays, cells were assayed in Seahorse DMEM base media containing 2 mM glutamine using sequential injections of 10 mM glucose, 1 μ M oligomycin, and 50 mM 2-deoxyglucose.

For each Seahorse plate, CyQuant (Life Technologies) was used to normalize measurements to cell number/well. For both mitochondrial stress assays and glycolysis stress assays, calculations were made from an average of the three measurement points per cycle. Basal mitochondrial respiration was calculated from the average OCR prior to inhibitor addition, while maximal respiration was calculated from the average OCR following oligomycin addition. Cellular glycolysis represents the average ECAR following glucose addition, maximal glycolytic capacity represents average ECAR following oligomycin injection, and glycolytic reserve was calculated as the difference between the glycolytic capacity and cellular glycolysis.

ATP Synthesis Assays. ATP synthesis rates were measured essentially as described (34) in replicate 10- μ g aliquots of freshly harvested Flp-InTM T-RexTM 293 cells. Samples were permeabilized with 50 μ g/mL digitonin in ATP assay buffer (25 mM Tris, 150 mM KCl, 2 mM EDTA, 10 mM K₂HPO₄, pH 7.4) containing 1 mM ADP and indicated substrate/inhibitor concentrations (10 mM succinate; 10 mM glutamate; 10 mM malate; 10 mM pyruvate; 2.5 μ M rotenone; 1 mM malonate). Samples were incubated at 37°C for 20 min, then stopped by the addition of perchloric acid on ice. The ATP concentration of neutralized samples was measured in a microplate reader using an ATP Bioluminescence Assay Kit CLS II (Roche, 11699695001). ATP synthesis rates were calculated from triplicate assays and reported as nmol ATP/mg protein/min.

Quantitative MS and Data Analysis. Quantitative MS of isolated mitochondria was performed exactly as described previously in Jackson et al. (4, 35, 36). For a detailed description of the processing of IP eluates, analysis of all samples by quantitative MS, and processing and visualization of MS data, see *SI Appendix*.

OXPLOS plots were generated as described previously (4, 37). Topographical mapping of log₂-transformed label-free quantitation (LFQ) intensities to the complex I structure (Protein Data Bank [PDB] 5LDW) was performed using python scripts as described previously (36).

Complexome Profiling. For stable isotope labeling with amino acids in cell culture (SILAC) labeling, control and SFXN4^{KO} HEK Flp-In cells were cultured in "light" or "heavy" (containing ¹³C₆¹⁵N₄-arginine and ¹³C₆¹⁵N₂-lysine) SILAC DMEM. Mitochondria were isolated from both cell lines using the previously described procedure, before 100 μg mitochondria from each cell line were combined and solubilized at 2 mg/mL in 1% digitonin-containing solubilization buffer (20 mM Bis-Tris, 50 mM NaCl, 10% [vol/vol] glycerol, pH 7.4, 1% [wt/vol] digitonin). Solubilization was allowed to occur on ice for 30 min, before insoluble material was removed through centrifugation at 16,000 × g for 30 min. BN loading dye (0.5% [wt/vol] Coomassie blue G250, 50 mM ε-amino n-caproic acid, 10 mM Bis-Tris, pH 7.0) was added to the clarified supernatant prior to loading. Digitonin-solubilized mitochondria were processed via BN-PAGE using a 4–13% acrylamide gradient gel, which was run overnight. The BN-PAGE gel was subsequently processed sliced into 60 even slices for analysis by MS. For a detailed description of the subsequent processing, analysis, and visualization of the complexome data, see *SI Appendix*.

Data Availability. All study data are included in the article and/or supporting information. We have supplied entire unfiltered datasets for all proteomics experiments as supplementary materials. The mass spectrometry proteomics

data have been deposited to the ProteomeXchange Consortium via the PRIDE partner repository with the dataset identifier [PXD032762](https://doi.org/10.1093/bioinformatics/btad000).

ACKNOWLEDGMENTS. We acknowledge support from the Mito Foundation to Stojanovski Lab (Incubator and Booster Grant). T.D.J., J.J.C., and K.M.F. are supported by Australian Government Research Training Program scholarships. D.H.H. is supported by a Melbourne International Research Scholarship. T.D.J., J.J.C., and D.H.H. are supported by Mito Foundation PhD Top-Up scholarships. We acknowledge funding from the Australian National Health and Medical Research Council (NHMRC Project Grant GNT1140906 to D.A.S. and M.T.R.; GNT1107094 to D.R.T.; NHMRC Fellowship 1140851 to D.A.S.; 1155244 to D.R.T.; EL1 Investigator Grant APP2010149 to L.E.F.). We thank the Bio21 Mass Spectrometry and Proteomics Facility for the provision of instrumentation, training, and technical support and the Mito Foundation for a large equipment grant supporting proteomics infrastructure. L.E.F. acknowledges support from the Mito Foundation. A.E.F. and D.R.T. acknowledge additional support from the Mito Foundation and the Victorian Governments Operational Infrastructure Support Program.

Author affiliations: ^aDepartment of Biochemistry and Pharmacology, The University of Melbourne, Parkville, VIC 3010, Australia; ^bBio21 Molecular Science and Biotechnology Institute, The University of Melbourne, Parkville, VIC 3010, Australia; ^cMurdoch Children's Research Institute, Royal Children's Hospital, Melbourne, VIC 3052, Australia; ^dDepartment of Paediatrics, University of Melbourne, Melbourne, VIC 3052, Australia; ^eDepartment of Biochemistry and Molecular Biology, Monash Biomedicine Discovery Institute, Monash University, Clayton, VIC 3168, Australia; ^fDivision of Cancer Research, Peter MacCallum Cancer Centre, Melbourne, VIC 3000, Australia; ^gSir Peter MacCallum Department of Oncology, The University of Melbourne, Parkville, VIC 3010, Australia; and ^hVictorian Clinical Genetic Services, Royal Children's Hospital, Melbourne, VIC 3052, Australia

1. A. J. Anderson, T. D. Jackson, D. A. Stroud, D. Stojanovski, Mitochondria-hubs for regulating cellular biochemistry: Emerging concepts and networks. *Open Biol.* **9**, 190126 (2019).
2. S. Rath et al., MitoCarta3.0: An updated mitochondrial proteome now with sub-organelle localization and pathway annotations. *Nucleic Acids Res.* **49** (D1), D1541–D1547 (2021).
3. A. Y. Sung, B. J. Floyd, D. J. Pagliarini, Systems biochemistry approaches to defining mitochondrial protein function. *Cell Metab.* **31**, 669–678 (2020).
4. T. D. Jackson et al., The TIM22 complex mediates the import of sideroflexins and is required for efficient mitochondrial one-carbon metabolism. *Mol. Biol. Cell* **32**, 475–491 (2021).
5. N. Kory et al., SFXN1 is a mitochondrial serine transporter required for one-carbon metabolism. *Science* **362**, eaat9528 (2018).
6. M. G. Acoba et al., The mitochondrial carrier SFXN1 is critical for complex III integrity and cellular metabolism. *Cell Rep.* **34**, 108869 (2021).
7. G. J. Hildick-Smith et al., Macrocytic anemia and mitochondriopathy resulting from a defect in sideroflexin 4. *Am. J. Hum. Genet.* **93**, 906–914 (2013).
8. K. Sofou et al., Prenatal onset of mitochondrial disease is associated with sideroflexin 4 deficiency. *Mitochondrion* **47**, 76–81 (2019).
9. L. E. Formosa, M. G. Dibley, D. A. Stroud, M. T. Ryan, "Building a complex complex: Assembly of mitochondrial respiratory chain complex I" in *Seminars in Cell & Developmental Biology* (Elsevier, 2018), pp. 154–162.
10. L. Sánchez-Caballero, S. Guerrero-Castillo, L. Nijtmans, Unraveling the complexity of mitochondrial complex I assembly: A dynamic process. *Biochim. Biophys. Acta* **1857**, 980–990 (2016).
11. H. Heide et al., Complexome profiling identifies TMEM126B as a component of the mitochondrial complex I assembly complex. *Cell Metab.* **16**, 538–549 (2012).
12. L. E. Formosa et al., Dissecting the roles of mitochondrial complex I intermediate assembly complex factors in the biogenesis of complex I. *Cell Rep.* **31**, 107541 (2020).
13. S. Guerrero-Castillo et al., The assembly pathway of mitochondrial respiratory chain complex I. *Cell Metab.* **25**, 128–139 (2017).
14. J. G. Fedor, J. Hirst, Mitochondrial supercomplexes do not enhance catalysis by quinone channeling. *Cell Metab.* **28**, 525–531.e524 (2018).
15. E. Lapuente-Brun et al., Supercomplex assembly determines electron flux in the mitochondrial electron transport chain. *Science* **340**, 1567–1570 (2013).
16. M. Protasoni et al., Respiratory supercomplexes act as a platform for complex III-mediated maturation of human mitochondrial complexes I and IV. *EMBO J.* **39**, e102817 (2020).
17. J. M. Dempster et al., Extracting biological insights from the Project Achilles genome-scale CRISPR screens in cancer cell lines. *BioRxiv* [Preprint] (2019). <https://www.biorxiv.org/content/10.1101/720243v1>. Accessed 20 August 2020.
18. R. M. Meyers et al., Computational correction of copy number effect improves specificity of CRISPR-Cas9 essentiality screens in cancer cells. *Nat. Genet.* **49**, 1779–1784 (2017).
19. B. T. Paul, L. Tesfay, C. R. Winkler, F. M. Torti, S. V. Torti, Sideroflexin 4 affects Fe-S cluster biogenesis, iron metabolism, mitochondrial respiration and heme biosynthetic enzymes. *Sci. Rep.* **9**, 19634 (2019).
20. N. Maio, T. A. Rouault, Outlining the complex pathway of mammalian Fe-S cluster biogenesis. *Trends Biochem. Sci.* **45**, 411–426 (2020).
21. S. Guerrero-Castillo, J. van Strien, U. Brandt, S. Arnold, Ablation of mitochondrial DNA results in widespread remodeling of the mitochondrial complexome. *EMBO J.* **40**, e108648 (2021).
22. E. Perales-Clemente et al., Five entry points of the mitochondrially encoded subunits in mammalian complex I assembly. *Mol. Cell Biol.* **30**, 3038–3047 (2010).
23. C. Wang et al., MITRAC15/COA1 promotes mitochondrial translation in a ND2 ribosome-nascent chain complex. *EMBO Rep.* **21**, e48833 (2020).
24. D. R. Richardson et al., Mitochondrial iron trafficking and the integration of iron metabolism between the mitochondrion and cytosol. *Proc. Natl. Acad. Sci. U.S.A.* **107**, 10775–10782 (2010).
25. N. P. Mena, A. L. Bulteanu, J. Salazar, E. C. Hirsch, M. T. Núñez, Effect of mitochondrial complex I inhibition on Fe-S cluster protein activity. *Biochem. Biophys. Res. Commun.* **409**, 241–246 (2011).
26. B. Andrews, J. Carroll, S. Ding, I. M. Fearnley, J. E. Walker, Assembly factors for the membrane arm of human complex I. *Proc. Natl. Acad. Sci. U.S.A.* **110**, 18934–18939 (2013).
27. V. Guarani et al., TIMMDC1/C3orf1 functions as a membrane-embedded mitochondrial complex I assembly factor through association with the MCIA complex. *Mol. Cell Biol.* **34**, 847–861 (2014).
28. V. Žárský, P. Doležal, Evolution of the Tim17 protein family. *Biol. Direct* **11**, 54 (2016).
29. S. S. Shinde, S. Sharma, L. Teekas, A. Sharma, N. Vijay, Recurrent erosion of COA1/MITRAC15 demonstrates gene dispensability in oxidative phosphorylation. *bioRxiv* (2021).
30. Y. Kang et al., Function of hTim8a in complex IV assembly in neuronal cells provides insight into pathomechanism underlying Mohr-Tranebjærg syndrome. *eLife* **8**, e48828 (2019).
31. K. Labun et al., CHOPCHOP v3: expanding the CRISPR web toolbox beyond genome editing. *Nuc. Acids Res.* (2019).
32. H. Schägger, G. von Jagow, Tricine-sodium dodecyl sulfate-polyacrylamide gel electrophoresis for the separation of proteins in the range from 1 to 100 kDa. *Anal. Biochem.* **166**, 368–379 (1987).
33. A. E. Frazier, A. E. Vincent, D. M. Turnbull, D. R. Thorburn, R. W. Taylor, Assessment of mitochondrial respiratory chain enzymes in cells and tissues. *Methods Cell Biol.* **155**, 121–156 (2020).
34. M. J. Bird et al., Neuronal and astrocyte dysfunction diverges from embryonic fibroblasts in the Ndufs4fky/fky mouse. *Biosci. Rep.* **34**, e00151 (2014).
35. N. A. Kulak, G. Pichler, I. Paron, N. Nagaraj, M. Mann, Minimal, encapsulated proteomic-sample processing applied to copy-number estimation in eukaryotic cells. *Nat. Methods* **11**, 319–324 (2014).
36. D. A. Stroud et al., Accessory subunits are integral for assembly and function of human mitochondrial complex I. *Nature* **538**, 123–126 (2016).
37. N. J. Lake et al., Biallelic mutations in MRPS34 lead to instability of the small mitoribosomal subunit and Leigh syndrome. *Am. J. Hum. Genet.* **101**, 239–254 (2017).